

MODELING OF CLIMBING ROBOTS ON NON-PLANAR SURFACES

PADMANABHAN KUMAR, STEPHEN L CANFIELD, JOSHUA QUALLS

Department of Mechanical Engineering, Tennessee Technological University, Cookeville TN, 38505, USA,
SCANfield@tntech.edu

INTRODUCTION

Mobile robots capable of climbing provide a platform which can be used to perform a large variety of inspection, manufacturing and or maintenance tasks. Examples of these tasks include welding, painting, and inspection, [1-4]. Mobile robots offer the ability to automate routine tasks traditionally relying on difficult manual labor. They also provide the ability to perform manufacturing or maintenance tasks remotely which can reduce the possibility of hazardous exposure to humans and thus reduce safety concerns when working in environments considered harmful or toxic by nature. This is of significant interest to members of the nuclear industry requiring ongoing maintenance, where repair of equipment subject to environmental effects can be hazardous to humans.

While there has been research and developmental to create and test remote mobile climbing robotic systems, these devices are almost always based on underlying design models assuming operation on planar surfaces. However, in practice, very few structures are actually planar and better characterized by non-planar surfaces, both at local scale (obtrusions, local features) and a global scale (structures with non-planar geometric shapes such as cylinders, spheres, etc). The desired operations for these mobile robots generally require controlled tracking of specified paths or trajectories to complete the maintenance or manufacturing task. Often, the surfaces encountered in a nuclear power production or storage environment can be modeled as common geometric shapes such as cylinders or spheres. One such example is the dry canister storage system (DCSS) which is used for storing spent nuclear fuel. These surfaces have a generally known geometry which can be incorporated into the robot motion prediction model. The robot configuration must accurately adapt to the surface and these effects must be considered in the robot kinematic and/or dynamic model to maintain desired motion performance. Thus, incorporating non-planar effects into the kinematic considerations for mobile robot design and analysis is important to drive the design of viable remote systems in the future.

The purpose of the current work is to summarize and demonstrate the ability of a model to approximate the position and orientation of a mobile robotic platform while it navigates a cylindrical climbing surface representing typical storage containers used in the nuclear power industry. The result is to provide improved performance in localization and motion tracking for performing inspection and maintenance tasks.

APPROACH

The literature presents a limited number of models to consider robot operation on non-planar surfaces. These methods are primarily focused on non-slip behavior, vehicle topology modification required. Use of differential expression of kinematic contact equations based on [5] is presented in [3, 6-8], with algebraic Kinematic models for non-planar operation demonstrated in [3, 8-9]. Of these, [3, 9] directly discuss application to climbing systems. This paper will compare these two models (differential kinematic equations and algebraic kinematic model) based on their ability to approximate the position and orientation of a mobile robotic platform while it navigates a cylindrical climbing surface representing typical storage containers used in the nuclear power industry. The models will be compared based on robust prediction and computational effort required. The first model provides an algebraic description of the mobile robot kinematics on cylindrical surfaces and assumes a skid-steer configuration with the necessary suspension to accommodate non-planar surface

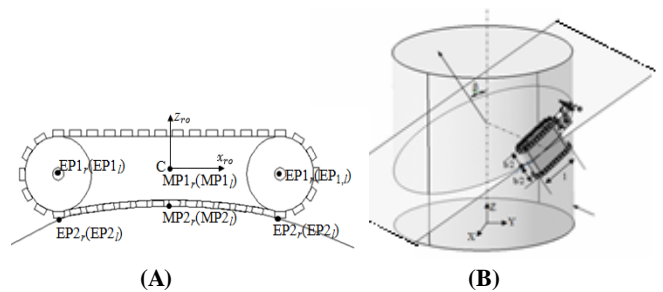


Figure 1: A.) Skid Steer Suspension B.) Climbing Surface

The model first assumes the robot traverses paths on cylindrical surfaces defined as the intersection of a plane (oriented by β) with the cylinder resulting in its position defined by sinusoidal curves. The orientation of the robot and its left and right robot tracks is provided through a process called geometric stability which distributes the non-planar displacements uniformly about the robot. This provides a set of algebraic equations as functions of the local surface normal requiring local iteration at each discrete point along the path to determine orientation.

The second model assumes point contact through a three wheeled differential steer platform traveling along a cylindrical surface on a defined path.

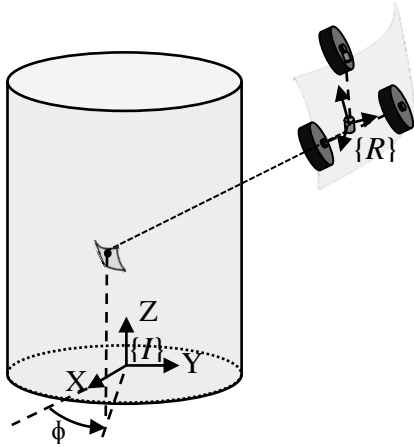


Figure 2: Climbing Surface and Robot

In addition, the second model uses a set of five differential equations to describe the motion of each contact point locally on the surface as a function of the relative velocity between the vehicle and surface with updates required for the configuration parameters. This yields a system of differential algebraic equations to be solved numerically along the path.

The models are constructed as follows:

The first model incorporates a tracked skid steer platform with width dimension labeled b and the length dimension labeled l . The climbing surface will be modeled as an upright cylinder with surface radius R_c . The left and right tracks will be separated by an equal offset of $\pm b/2$ from the center of the robot chassis and maintain contact with the cylindrical climbing surface of radius R , at location ϕ along the surface. The robotic platform traverses along the cylindrical climbing surface with the resulting trajectory unfolding along a sinusoidal curve described in, [10].

$$u(x) = R_c \tan(\beta) \sin\left(\frac{R_c \phi}{R_c}\right) + C_i \quad (1)$$

The relative lateral slip between the left and right tracks is estimated by the calculation of the track center distance at any location along the path as,

$$b_x = b * \cos\left(\text{atan}\left(R_c \tan(\beta) \cos\left(\frac{R_c \phi}{R_c}\right)\right)\right) \quad (2)$$

Geometric stability is then incorporated into the model by placing the robot on climbing surface in a manner allowing for the contact points of each track to be equally displaced from the surface. A set of line segments are then drawn creating mirrored triangles which are used to determine the position of the tracks. This begins by finding contact point $\mathbf{MP1}_i$, located at $\mathbf{MP1}_i = \mathbf{C} + \text{sign}(i) \frac{b}{2} \mathbf{y}_r$. The contact points $\mathbf{MP2}_i$ are then determined by extending a line from the contact point $\mathbf{MP1}_i$ to the climbing surface. Finally, the geometric triangle is finished by extending a line segment from $\mathbf{MP2}_i$ to the robots centroid, \mathbf{C} .

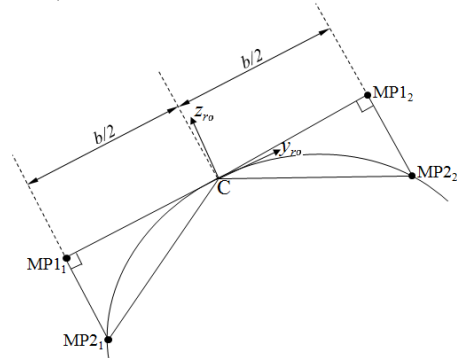


Figure 3a: rotation about x_{r0}

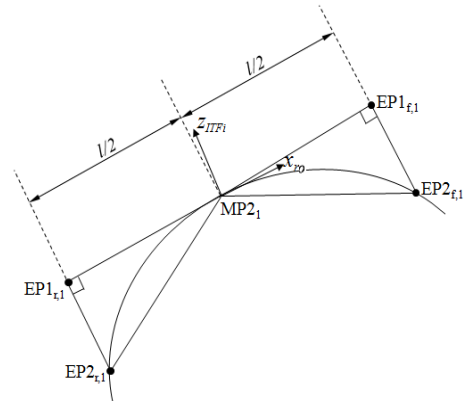


Figure 3b: rotation about y_l

This geometric triangle is then rotated about the robot frames x axis until the triangles $\mathbf{C-MP1}_1\text{-MP2}_1$ and $\mathbf{C-MP1}_2\text{-MP2}_2$ become mirrored achieving geometric stability for the robot tracks roll axis, Figure 3a. The process is then repeated at an intermediate track frame defined where z_l is the surface normal at $\mathbf{MP2}_i$ and y_l completes the frame. The contact points $\mathbf{EP1}_{r,i}$ and $\mathbf{EP2}_{r,i}$ are then

determined by extending a line from $\mathbf{MP2}_i$ to the contact point $\mathbf{EP1}_{r,i}$ and $\mathbf{EP2}_{r,i}$ is determined by extending a line from the contact point $\mathbf{EP1}_{r,i}$ to the climbing surface. Finally, the geometric triangle is finished by extending a line segment from $\mathbf{EP2}_{r,i}$ to $\mathbf{MP2}_i$. The line segment $\mathbf{EP1}_{r,i}$ - $\mathbf{EP1}_{f,i}$ is rotated about the y axis in the intermediate track frame until the triangles $\mathbf{MP2}_i$ - $\mathbf{EP1}_{f,i}$ - $\mathbf{EP2}_{f,i}$ and $\mathbf{MP2}_i$ - $\mathbf{EP1}_{r,i}$ - $\mathbf{EP2}_{r,i}$ become mirrored achieving stability for the tracks about the pitch axis, Figure 3b. This process is repeated at each discrete point along the path thus generating an updated path .

The second model uses a kinematic description for the robotic system and implements a method to propagate the wheel contact locations forward in time. The instantaneous model of the robot is developed from three in-parallel serial branches. This results in three wheel branches, left, right and caster. The left and caster wheel branch is 5 degrees of freedom and the right wheel branch is four degrees of freedom. This results in a set of three Jacobian matrices relating the velocity of the robot chassis $\{V_r\}$ to the configuration state velocity for each wheel branch as:

$$\mathbf{v}_r = \mathbf{J}_L \dot{\mathbf{q}}_L = \mathbf{R}_R^L \mathbf{J}_R \dot{\mathbf{q}}_R = \mathbf{R}_C^L \mathbf{J}_C \dot{\mathbf{q}}_C \quad (3)$$

with \mathbf{R}_R^L , \mathbf{R}_C^L representing the adjoint transformations that project velocity of the right and caster contact point frame into the left contact point frame. The vector of joint parameters for each of the three wheel branch is represented as

$\mathbf{q}_i = [\theta_1 \ \theta_2 \ \theta_3 \ \theta_4 \ \theta_5]^T_i$ with \mathbf{q}_i containing θ_{1-5} for $i =$ left and caster wheels, and θ_{1-4} for $i =$ right wheel, allowing the configuration velocities $\dot{\mathbf{q}}_i$, to be solved as,

$$\dot{\mathbf{q}}_L = \mathbf{J}_L^+ \mathbf{v}_r; \dot{\mathbf{q}}_R = (\mathbf{R}_R^L \mathbf{J}_R)^+ \mathbf{v}_r; \dot{\mathbf{q}}_C = (\mathbf{R}_C^L \mathbf{J}_C)^+ \mathbf{v}_r \quad (4)$$

These equations assume instantaneously fixed wheel contact locations which are propagated forward in time. This is achieved by satisfying the kinematic constraint equation using two defined inputs, \mathbf{q}_L (4) and \mathbf{q}_R (4), which are found by integrating Equation 4. Finally, the remaining 12 configuration parameters in \mathbf{q}_L , \mathbf{q}_R , and \mathbf{q}_C are determined as the set that satisfies equality of the three homogenous transformations, (left, right, and caster wheels). This method then employs a set of functions which characterizes the contacting surfaces as described in, [8], resulting in a set of five differential equations to describe the motion of contact points between the tracks and the climbing surface. The contact equations described the motion of the contact point on the wheel surface, $\dot{\mathbf{U}}_W = [\dot{u}_W \ \dot{v}_W]^T$, and the motion of the contact point on the climbing surface, $\dot{\mathbf{U}}_S = [\dot{u}_S \ \dot{v}_S]^T$ as:

$$\dot{\mathbf{U}}_W = \mathbf{M}_W^{-1} (\mathbf{K}_W + \bar{\mathbf{K}}_S)^{-1} \begin{bmatrix} -\omega_y \\ \omega_x \end{bmatrix} - \bar{\mathbf{K}}_S \begin{bmatrix} v_x \\ v_y \end{bmatrix} \quad (5)$$

$$\dot{\mathbf{U}}_S = \mathbf{M}_S^{-1} \mathbf{R}_W^S (\mathbf{K}_W + \bar{\mathbf{K}}_S)^{-1} \begin{bmatrix} -\omega_y \\ \omega_x \end{bmatrix} - \mathbf{K}_W \begin{bmatrix} v_x \\ v_y \end{bmatrix} \quad (6)$$

$$\dot{\psi} = \omega_z + \mathbf{T}_W \mathbf{M}_W \dot{\mathbf{U}}_W + \mathbf{T}_S \mathbf{M}_S \dot{\mathbf{U}}_S \quad (7)$$

where $\dot{\psi}$ is the rotation between the wheel and surface frames, \mathbf{R}_W^S is the orientation of the wheel frame projected on the surface frame, and $\bar{\mathbf{K}}_S$ is the curvature of the surface, at the point of contact and relative to the wheel,

$$\bar{\mathbf{K}}_S = \mathbf{R}_W^S{}^T \mathbf{K}_S \mathbf{R}_W^S \quad (8)$$

With the rotational and linear velocities described as $[-\omega_y \ \omega_x]^T = [-\mathbf{q}(2) \ \mathbf{q}(1)]^T$ and $[-v_x \ v_y]^T = [0 \ 0]^T$ due to the no-slip wheel assumptions.

The models are then used to develop simulations of configuration parameter behavior and expected path navigation. The model results are then compared with experimental data recorded from a developed robot chassis in order to determine the accuracy of the model in relation to experimental data.

RESULTS

A simplified test platform representing a skid-steer mobile robot was developed with magnetic tracks allowing for adhesion to the climbing surface. The platform was constructed with dimensions as follows: $b = 0.2032$ meters, $l = 0.2286$ meters. The platform itself was encoded to measure chassis suspension parameters, roll and pitch, between the two tracks while traversing a cylindrical surface. The roll and pitch measurements are encoded using 2500 count encoders and recorded through a Measurement Computing 8-Channel Quadrature Encoder using MATLAB software.

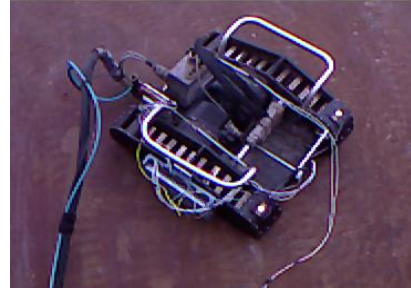


Figure 4: Skid Steer Robot Traversing Climbing

The roll and pitch data is collected as the robot traverses a set of desired paths around the cylindrical steel tank. The three paths traveled were at inclinations of 30, 60 and 80 degrees. The results presented below are based on the geometric stability model with a separate set of data being overlaid to represent the experimentally collected roll and pitch data. The experimental results presented are based on the three candidate paths described above, with non-dimensionalized robot parameters $l' = 0.3$, and $b' = 0.4$. Where $l' = l/R$ is the non-dimensionalized length and $b' = b/R$ the non-dimensionalized width.

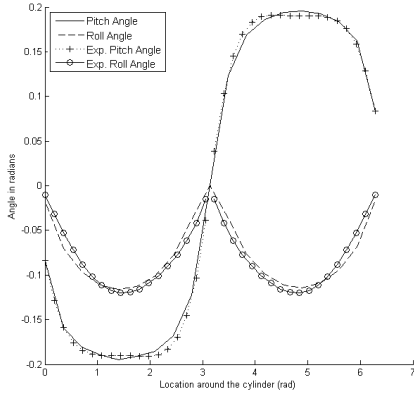


Figure 5a: Plot of pitch, yaw, and roll over the path $\beta = 30$ deg.

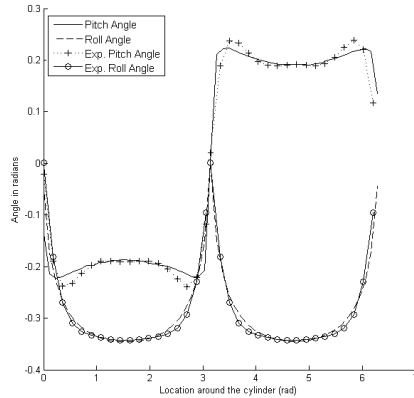


Figure 5b: Plot of pitch, yaw, and roll over the path $\beta = 60$ deg.

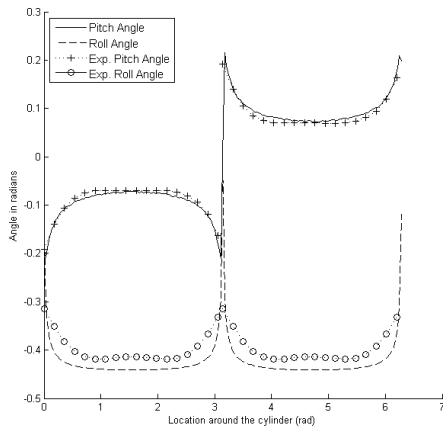


Figure 5c: Plot of pitch, yaw, and roll over the path $\beta = 80$ deg.

The above figures display a correlation between the model-predicted and experimental pitch and roll. The average error for each path is calculated, Table 1, in order to provide a measure of accuracy between the model and experimentation. The model indicates a

stronger correlation for paths at an inclination of 30 and 60 degrees with a slightly larger data differentiation with the path of 80 degrees.

Table 1: Pitch and Roll Candidate Path Error

Candidate Path	Pitch (% Error)	Roll (% Error)
30	1.7	0.9
60	2.2	1.8
80	6.4	7.1

The two independent models are then compared by generating a desired path that each robot model must navigate. The path is generated from the intersection of a plane at an inclination of 30 degrees with the cylindrical climbing surface. The vertical axis is the elevation along the climbing surface and the horizontal axis is the arc length of the unwrapped cylindrical surface represented as $R\phi$.

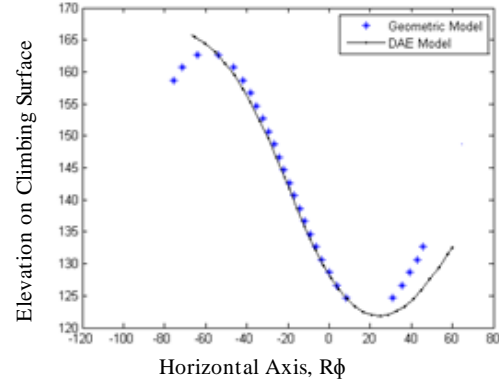


Figure 6: Path on Unwrapped Surface

It can be seen from the above figure both robots travel a path described by a sinusoidal function, as proposed earlier in this literature. The figure above does indicate some slight differences between the two models, with a maximum square error of 0.1404 m between the two simulated paths.

DISCUSSION

The presented methods discussed in this paper are used to evaluate mobile robot trajectory when traveling a non-planar surface. The two approaches differ in construction with the first method using geometric stability resulting in purely algebraic equations while the second method results in a motion description of the contact point between two surfaces yielding a set of ordinary differential equations. These equations combined with kinematic constraints are used to iteratively update the robots position. The primary purpose of the preceding work is to provide a means for advanced kinematic

modeling and path planning of mobile robots that navigate along non-planar surfaces.

The data shown in Figures 5a-c, in the previous section describe the behavior of the roll and pitch rotations between the left and right axes while traveling along three predetermined paths at inclinations of 30, 60, and 80 degrees. The data collected by model simulations was overlaid with experimentally collected pitch and roll data for comparison between the empirical and experimental data. The figures provide visual evidence this model provides accurate description of the roll and pitch when compared to the experimentally collected data. There are slight variations between the model and experimental results most likely resulting from the rotary encoders experiencing disturbances due to surface conditions. The results do however indicate the model prediction provides reasonable accuracy for the roll and pitch, with the most accurate representations occurring for paths with lower inclinations. The two models are then compared by estimation of robot travel along a predefined path. The expected path of the robot is determined by the intersection of a plane with the cylindrical climbing surface, thus confirming the path resembles a sinusoidal wave, Figure 6. While the two approaches differ in method the resulting paths are similar in nature with a maximum square error of 0.1404 meters. The error between the two curves could be attributed to factors such as integration technique or model configuration parameters.

CONCLUSION

The primary purpose of the work presented is to develop a means to accurately model and estimate the pose and position of mobile robots while navigating non-planar surfaces. The geometric model assumes the robotic platform undergoes a uniform distribution of the suspension as it navigates the surface, incorporating a set of algebraic equations to solve for the position and pose of the robot. The second model uses kinematic constraints and a set of differential algebraic equations to solve for location along the surface. Each model provides an accurate path representation while traversing the surface and can be used to provide trajectory estimation before performing service tasks. The ability to determine trajectory patterns on non-planar surfaces is increasingly desired in environments such as those which contain safety concerns like nuclear depositories, for instance. Through improvements in kinematic modeling there exists a possibility in reducing the reliance on devices such as cameras and laser navigation systems when working in harmful environments.

REFERENCES

1. Canfield, S. L. et al. "Robotic inspection in power plants." *ISA 51st Annual Instrumentation Symposium*. 2005
2. O'Toole, A and Canfield, S.L. "Developing a Kinematic Estimation Model for a Climbing Mobile Robotic Welding System," *Proc. of the 2010 ASME International Design Engineering Technical Conferences*, Montreal Quebec, Canada, Aug. 15-18, 2010, DETC2010-28878.
3. Qualls, J., Canfield, S.L., Hill, T., Shibakov, A. "Kinematic Analysis of a Mobile Robot Performing Manufacturing Tasks on Non-Planar Surfaces." *Proc. 2015 ASME. 39th Mechanisms and Robotics Conference*, Boston, MA. August 02-05, 2015
4. Canfield, S.L., Qualls, J., and Shibakov, A. "Kinematic and Dynamic Evaluation of Mobile Robots Performing Welding Tasks." *Proc. of the 2014 ASME International Design and Engineering Technical conferences*, Buffalo, N.Y. Aug 17-20, 2014.
5. Montana, D.J. The kinematics of contact and grasp, *Int. J. Rob. Res.* 7 (3) (1988) 17–32.
6. Chakraborty, N. Ghosal, "A. Kinematics of wheeled mobile robots on uneven terrain", *Mechanism and Machine Theory* 39 (2004) 1273-1287
7. Sarkar, N. and Kumar, V. "Control of Mechanical Systems With Rolling Constraints Application to Dynamic Control of Mobile Robots," *The International Journal of Robotics Research* 13.1 (1994): 55-69.
8. Grand, Christophe, Faiz Benamar, and Frédéric Plumet. "Motion kinematics analysis of wheeled-legged rover over 3D surface with posture adaptation." *Mechanism and Machine Theory* 45.3 (2010): 477-495.
9. P. Kumar, T. Hill, D. A. Bryant and S. L. Canfield, Modeling and design of a linkage-based suspension for tracked-type climbing mobile robotic systems, in *Proc. ASME 2011 International Design Engineering Technical Conferences*, DETC2011-48555, pp. 827-834 (2011)
10. T. M. Apostol and M. A. Mnatsakanian, Unwrapping Curves from Cylinders and Cones, *The Mathematical Association of America*, Monthly 114, May, (2007)